Energy & Buildings 307 (2024) 113976

Contents lists available at ScienceDirect

Energy & Buildings

journal homepage: www.elsevier.com/locate/enb

Impact of thermal control by real-time PMV using estimated occupants personal factors of metabolic rate and clothing insulation

Eun Ji Choi, Ji Young Yun, Young Jae Choi, Min Chae Seo, Jin Woo Moon *

School of Architecture and Building Science, Chung-Ang University, 84, Heukseok-ro, Dongjak-gu, Seoul 06974, Republic of Korea

ARTICLE INFO

Keywords:
Thermal control
Thermal comfort
Predicted mean vote
Clothing insulation
Metabolic rate
Occupant centric control

ABSTRACT

To optimize thermal comfort for occupants' wellbeing and health care, it's essential to adjust heating and cooling systems in real-time based on occupants' thermal preferences. For this, personal factors affect individual thermal comfort, such as metabolic rate and clothing insulation, should be estimated in real-time. The aim of this research is introducing an intelligent model capable of estimating metabolic rate and clothing insulation values from indoor images, suitable for both single and multi-occupant scenarios. Additionally, a control algorithm considering a real-time predicted mean vote (PMV), was developed using the proposed model, and its implications for thermal comfort and energy efficiency were investigated. Utilizing advanced computer vision methodologies, the model achieved a remarkable 95% training accuracy, and its reliability was further validated through experimentation. Evaluations of the PMV-based algorithm underscored its efficacy in enhancing thermal comfort relative to conventional methods in both individual and multi-occupant settings. Conversely, energy use was contingent upon the personal factors. In group settings, the mode values of metabolic rate and clothing insulation were effective for determining a representative PMV. In conclusion, the real-time PMV-based control represents a pioneering approach to augment thermal comfort using actual occupant data, paving the way for a synergistic balance between comfort augmentation and energy saving.

1. Introduction

1.1. Background

The perception of comfort within indoor spaces is widely acknowledged as pivotal, directly impacting human wellbeing, quality of life, and the sustainable operations of buildings [1,2]. Efforts to provide a pleasant thermal environment have led to research that considers both passive and active technologies, including the development of high-performance building envelopes, building automation systems, and intelligent control systems [3,4]. Although building facility systems should prioritize creating a pleasant thermal environment, the systems are typically controlled based on a simple set temperature. Such control systems often neglect occupants' thermal comfort. This can precipitate overcooling or overheating, culminating in an adverse thermal environment and heightened energy consumption [5,6]. Consequently, there has been a shift from on/off controls based on indoor set temperatures to those focusing on comfort-driven building control [7].

To control buildings considering human thermal comfort, the Predicted Mean Vote (PMV), a representative thermal comfort model rooted in human thermal balance, has been utilized as a control variable [8]. The PMV is calculated as per Equation (1):

$$PMV = f(T_{air},\ T_{mrt},\ RH,\ V_{air},\ M,\ I_{cl}) \tag{1}$$

where T_{air} is the air temperature (°C), T_{mrt} is the mean radiant temperature (°C), RH is the relative humidity (%), V_{air} is the air velocity (m/s), M is the metabolic rate (W/m^2), and I_{cl} is the clothing insulation ($m^2 \bullet K/W$). Thus, the components influencing PMV consist of four environmental factors and two personal factors. Several research efforts utilizing PMV for indoor thermal control have demonstrated improved thermal comfort [9,10]. Although environmental variables are easily measurable, personal factors, despite their critical role in PMV calculations, are often assumed static values due to their dynamic characteristics and measurement difficulty [11,12].

Utilizing arbitrary personal factors can hinder the accurate representation of an occupant's genuine thermal comfort needs, potentially fostering an uncomfortable environment. This oversight may escalate into wasteful energy consumption from excessive heating and cooling

* Corresponding author.
E-mail addresses: ejjchl77@cau.ac.kr (E.J. Choi), yjyyjy5350@cau.ac.kr (J.Y. Yun), chldudwo13@cau.ac.kr (Y.J. Choi), minchae@cau.ac.kr (M.C. Seo), gilerbert73@cau.ac.kr (J.W. Moon).

https://doi.org/10.1016/j.enbuild.2024.113976
Received 18 September 2023; Received in revised form 15 January 2024; Accepted 31 January 2024
Available online 6 February 2024

Nomenclature

T_{air}	air temperature [°C]
RH	relative humidity [%]
T_{mrt}	mean radiant temperature [°C]
V_{air}	air velocity [m/s]
T_{set}	temperature set point [°C]
M	metabolic rate [met or W/m^2]
I_{cl}	clothing insulation [clo or m^2•K/W]
I_{clu}	garment insulation [clo or m^2•K/W]

Abbreviation

PMV	Predicted Mean Vote
TSV	Thermal Sensation Vote
BMI	Body Mass Index (kg/m^2)
OCC	Occupant-Centric Control
MET subnet	Metabolic rate subnet
CLO subnet	Clothing insulation subnet
DNN	Deep Neural Network
CNN	Convolutional Neural Network
B-box	Bounding-box
IEA	International Energy Agency
MAE	Mean Absolute Error
FPS	Frames Per Second
IR	Infrared
HVAC	Heating, Ventilation and Air Conditioning
AC	Air Conditioning
COP	Coefficient of Performance
PCS	Personal Comfort System

system operations. Hence, the emphasis has been placed on the importance of a thermal control strategy rooted in PMV, considering the actual metabolic rate and clothing insulation values of occupants. Consequently, there has been a drive to devise robust methods for assessing and computing these personal factors.

1.2. Methodologies for measuring personal factors

To accurately measure personal factors, the use of high-end measurement equipment and the direct intervention of specialists are required. The complexity of this process and its limited field applicability make it challenging to implement in real-world scenarios. As a result, significant efforts have been channeled into devising methods that objectively and conveniently estimate these factors without the necessity for expert involvement. In the context of this research, henceforth, metabolic rate and clothing insulation will be denoted by the abbreviations M and I_{cl}, respectively.

Among personal factors, M represents the heat produced by human metabolic activity [11]. For estimating dynamic activity levels, primary parameters utilized have included 1) skin temperature, 2) heart rate, 3) respiration rate, and 4) behavior and posture. These parameters have mainly been measured using wearable devices such as smartwatches (e.g., Fitbit, Microsoft band) and smart bands (e.g., Polar H7 Strap) that track biometric data like heart rate and acceleration [13–15]. However, methods leveraging biometric data present challenges: they may not accurately gauge activity across all ranges [16,17], and they necessitate individuals to wear sensors or own specific measuring equipment. In terms of I_{cl}, it signifies the insulation value of the total clothing worn by an individual. Similar to M, the determination of I_{cl} values has predominantly relied on non-invasive sensors, focusing primarily on the measurements of skin and clothing surface temperatures. Some studies even resorted to attaching thermocouples and similar temperature-measuring sensors directly onto participants [18]. Nonetheless, such methods can cause discomfort to occupants. Practical challenges also arise in real-world settings, where every individual occupant would need to possess the required measuring equipment.

With the rapid progression of computer vision, recent approaches utilize deep learning-trained thermal and RGB images. These methodologies enable objective determination of M or I_{cl} values in real-world scenarios, reducing the need for user intervention [19–28]. Human pose estimation, which identifies joint key points from images, has been applied as a primary method for determining M values [19–23]. This approach encompasses the essential concept of classifying activities based on the movement patterns of human joints and estimating the corresponding activity levels. For I_{cl} estimations, research has leveraged thermal images, analyzing temperature differentials between clothing and skin [24,25]. Additionally, RGB images serve as essential variables in models designed to classify clothing based on attributes like type, material, and weight [26–29].

Vision technology has proven effective in real-time determination of an individual's M and I_{cl} values across various indoor settings, facilitating more accurate PMV calculations [30]. Assessments of thermal comfort should consider both M and I_{cl} concurrently. At present, there is limited research on real-time measurement of both values together, although a few recent studies have demonstrated the potential of thermal and RGB images for classifying activity and clothing [21–23]. Nevertheless, existing studies are constrained by the restricted range of personal factors they address and they focused solely on upper body clothing classification. Additionally, evaluations of models designed for multiple occupants are still inadequate. To overcome these limitations, there's a pressing need to develop real-time PMV optimization methods that can accurately determine occupants personal factors in both single- and multi-occupant settings.

1.3. Building control based on thermal comfort

Recent advancements in the field of occupant-centric control (OCC) have been geared towards balancing the dual objectives of ensuring occupant comfort and promoting efficient energy operations in buildings [31]. The International Energy Agency (IEA) emphasizes the importance of harnessing occupant data in refining building operations. Such integration not only elevates thermal comfort but also curtails unnecessary energy expenditures. It's worth noting that an individual's thermal comfort profoundly influences the 'preference' component, a fundamental aspect of OCC.

One of the primary objectives of estimating personal factors is to augment the precision of systems aiming for thermal comfort. Therefore, beyond merely developing methods to measure individual factors, it's imperative to ascertain the efficacy of building operations that can enhance occupant thermal comfort through system controls. However, there is limited research that experimentally evaluates the impact of implementing real-time personal factor estimation techniques within actual Heating, Ventilation, and Air Conditioning (HVAC) systems. Therefore, there's an imperative demand to apply real-time personal factor estimation in actual thermal controls to comprehensively evaluate its effects on both occupant thermal comfort and the associated energy use.

Furthermore, there is a noticeable gap in research focusing on thermal controls in multi-occupant settings. In real-world building scenarios aiming for optimal system control based on thermal comfort, a collective thermal preference of a group becomes indispensable. This preference should reflect the individual comforts of each occupant. As such, methods that center on real-time PMV-based controls present foundational technologies, making zone-specific HVAC operations

adaptable to individual occupants' needs.

1.4. Research purpose

Accurately measuring the personal factors (M and I_{cl}) of occupants in real-time and integrating them into building controls remains a significant challenge. The objective of this study is to evaluate the performance of a real-time PMV-based indoor thermal control system in terms of thermal comfort and energy efficiency, utilizing a model that estimates personal factors through computer vision technology. To address this, a comprehensive model designed to extract occupants M and I_{cl} values from indoor images has been introduced, which is applicable to both single and multi-occupant environments. Additionally, a control algorithm that incorporates real-time PMV values has been developed.

The main content presented in this study is as follows: (1) An advanced model has been developed that effectively estimates the personal factors of occupants, applicable for real-world building contexts. This model, which covers a range of indoor activities and clothing types, ensures high accuracy by detecting both upper and lower clothing simultaneously. (2) A systematic assessment has been conducted to understand the influence of HVAC systems, adjusted for thermal comfort, on both occupant thermal sensation and building energy consumption. (3) A novel approach has been proposed for determining a representative PMV value to optimize thermal comfort for the maximum number of occupants.

2. Methods

In this section, the methodology for estimating personal factors and real-time PMV-based building control is elaborated in detail. A comprehensive description of the experiment and conditions is provided, emphasizing the reliability of the experimental results.

2.1. The vision network for estimating personal factors

The development of models for estimating personal factors is still in the early stages of research. Common limitations in prior studies on measuring M and I_{cl} include inadequate applicability and certainty in real-world settings. Some studies focused on developing models for individual personal factors, lacking methods for estimating M and I_{cl} for multiple individuals. Additionally, generating diverse combinations of these two variables poses a challenge. In some studies, the number of selected combinations for estimating personal factors (e.g. four in total, two M × two I_{cl}) is limited and may not be sufficient for practical application. Specifically, regarding I_{cl}, all studies only included tops in classifiable garments. In real-world scenarios where multiple individuals and various variables can occur, creating a universally applicable model for the diverse personal factors of occupants remains challenging. Hence, this study developed an integrated intelligent model utilizing images as input variables to estimate real-time personal factors for individual occupants residing indoors.

The "Personal Factors estimation model" (hereafter referred to as PF model) was developed to collectively estimate occupants' M and I_{cl}. The structure of this model is illustrated in Fig. 1 and consists of a feature extraction phase and subnets phase that derive M and I_{cl} from the extracted features. During the feature extraction phase, information regarding the location of a person's joint key points, which is fundamental data for training, is extracted using human pose estimation techniques. This information is used to detect individual occupants, subsequently aiding in the assessment of presence and quantification of the number of occupants. Among various human pose estimation networks [32–34], OpenPose [35] network is employed, which is capable of recognizing the joints of multiple individuals simultaneously.

During the subnets phase, M and I_{cl} values for individual occupants are derived using the extracted key points information and the detected human image. The models, named MET subnet and CLO subnet, employ a Deep Neural Network (DNN) and a Convolutional Neural Network (CNN), respectively, for the classification of activity and clothing. The MET and CLO subnets were initially developed by our research team in prior work. Building on that foundation, each model was further advanced and integrated within the feature extraction phase. Consequently, a unified model capable of simultaneously estimating both personal factors was proposed.

Compared to previous studies, the distinctive characteristics of the PF model proposed in this research are as follows. First, the introduced methodology is designed to apply to multiple occupants. In the process, individuals are detected from the image, and based on each person's bounding-box (B-box) image, individual M and I_{cl} values are precisely estimated. This method, by distinguishing between individuals and mitigating interference from complex backgrounds, minimizes potential errors. Secondly, this study's model expands on the types of the M and I_{cl}, encompassing a broader range of activities and clothing combinations. The activities considered for estimating M in this model have been expanded to five categories, while individual clothing types for I_{cl} estimation have been broadened to 16 categories. Moreover, the I_{cl} value can be calculated in more than 34 combinations based on the mix of upper and lower clothing. Essentially, the number of possible M and I_{cl} combinations that can be jointly estimated has significantly expanded,

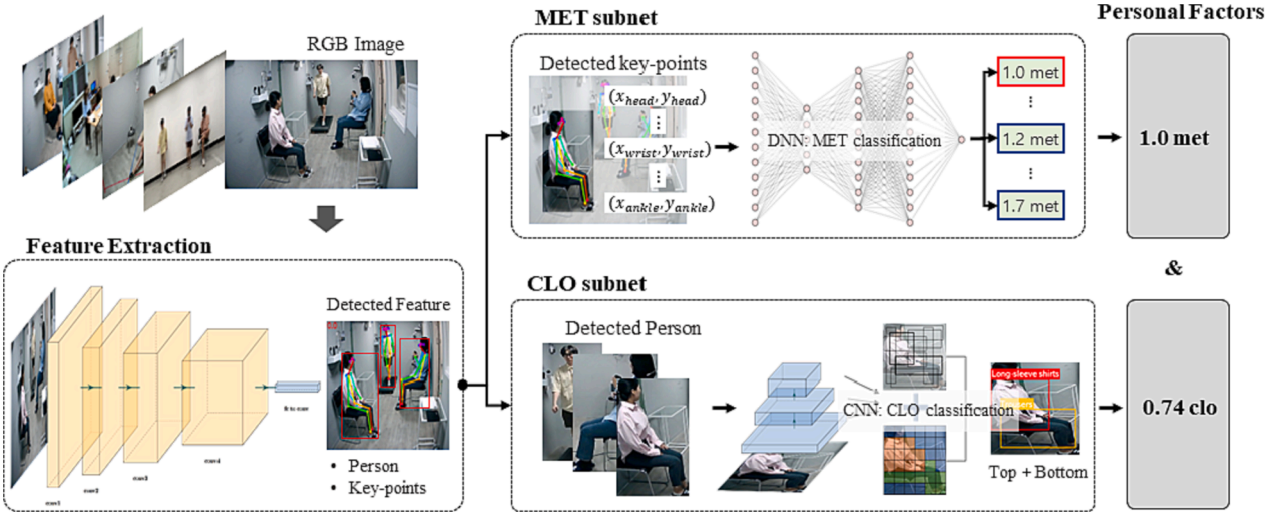

Fig. 1. Conceptual diagram of the PF model for estimating M and I_{cl}.

implying this approach as an advanced methodology with enhanced versatility and broad applicability.

The system platform utilized for model training consisted of an NVIDIA Quadro RTX 8000, Ubuntu 20.04 LTS, Python 3.9.0, CUDA 11.4, and PyTorch 1.8.1. The accuracy and applicability of the model were analyzed using a test dataset and a Test-bed. The model performance was analyzed using a confusion matrix, a tool commonly employed for evaluating the performance of classification models.

2.1.1. MET subnet

The MET subnet, structured as a DNN, processes input data from 18 pairs of detected key point coordinates (x, y) to classify activities and then outputs the corresponding M value. Utilizing joint coordinates for activity classification is a method grounded in well-established methodologies [19,23,36,37]. The joint details for the model are sourced from the information extracted during the feature extraction phase, and it categorizes five representative activities commonly encountered in indoor environments. Table 1 displays the activity types that can be classified, the M values corresponding to each activity, and the heat emission (W/m^2) from the human body associated with each activity [11]. Considering the indoor context, "Walking" is defined as a slow-paced activity at speeds below 2.5 km/h, while "Exercise" is restricted to indoor activities like yoga and calisthenics.

The MET subnet is composed of an input layer, three hidden layers, and an output layer. The input neurons consist of 36, each receiving x and y values of 18 joints, and it outputs a single M value. The primary parameters for the model include the ReLU activation function and the Adam optimization algorithm. The learning rate and tolerance were set at 0.01 and 1e-7, respectively. During model training, early stopping was implemented.

The MET subnet utilizes a distance threshold from joint coordinates acquired from previous image data to reflect the relevance with current data. Consequently, the more consecutive the image data, the more the error can be reduced. For continuous image training over time, images were stored at intervals of 1 s. Fig. 2 presents examples of collected training data categorized by activity. Images for training were directly acquired both online and from laboratory experiments, culminating in a total of 10,100 data points [38]. Efforts were made to minimize biases arising from the training data by diversifying the environments and camera angles during data collection.

2.1.2. CLO subnet

The CLO subnet was developed using the YOLOv5 [35] structure based on CNN which is capable of object detection and classification. As illustrated in Fig. 3, the CLO subnet discerns garments within the identified human B-box image and classifies the types of both upper and lower garments. The CLO subnet was developed in prior research [28] and offers the advantage of being able to freely combine garment types within the classifiable garments, enabling the estimation of various clothing levels. This approach is more realistic compared to existing methods that either classify the entire clothing combination as a fixed class or only classify the upper garment.

The developed CLO subnet is capable of classifying 16 garment types as proposed in ISO 9920 and ASHRAE standard 55. These garments are categorized into Top, Bottom, Outer, Dress, and Pajama. The types of garments corresponding to each category, along with their insulation of a garment (I_{clu}), are presented in Table 2. Training data was collected both online and offline, with a portion of the collected data being viewable in Fig. 4. The dataset includes full-body images reflecting individual garments and various clothing combinations. To minimize data bias, images were collected considering various angles, postures, and depth perceptions. The training dataset comprises 6,664 images, which were randomly divided into train (70 %), valid (10 %), and test (20 %) sets. The model underwent transfer learning based on a pre-trained YOLOv5 model [35]. The performance evaluation of the CLO subnet, akin to the MET subnet, utilized the confusion matrix to analyze such as accuracy, precision, and recall for each garment type.

Table 1
Activity types of MET subnet.

Activity	Metabolic rate	
	met	W/m^2
Sleeping	0.7	40
Sitting	1.0	60
Standing	1.2	70
Walking	1.7	100
Exercise	3.5	210

2.2. Real-time PMV-based control algorithm

A control algorithm, depicted in Fig. 5, was developed to control the indoor thermal environment using the PF model. The procedure of the algorithm is outlined below:

Step A represents the data acquisition phase, during which environmental data and RGB images are collected from compound sensor modules installed indoors. The environmental data encompasses factors such as T_{air}, RH, T_{mrt}, V_{air}, and system power consumption (W).

In Step B, individuals are identified, and their respective M and I_{cl} values are determined using the MET & CLO subnets detailed in Section 2.1. Initially, the collected images are examined to ascertain the presence of a person. If an individual is detected, the information from the extracted joint key points and the person's B-box image are directed to the MET and CLO subnets, respectively, yielding M and I_{cl} values. The gathered indoor environmental data, along with occupancy information, are saved in a database. This procedure is consistently repeated throughout the control cycle. In this study, the control cycle was set at 10 min intervals, demonstrating the potential for deriving personal factors that change over short periods. The control cycle is adjustable by administrators based on the building's purpose, conditions, and other factors.

Step C involves determining a representative single M and I_{cl} value for the control duration. While the mean value of indoor environmental data was utilized to represent the control period of 10 min, the mode was used for the personal factors. Using the established representative values, the current control cycle's PMV is calculated.

In Step D, the optimal set temperature (T_{set}) is determined to ensure that the PMV remains within the comfort range. The decision for the set value in Step D is guided by the feedback control logic presented in Fig. 6. The current PMV information is dispatched as a feedback signal. Subsequently, the deviation between the PMV setpoint and the current PMV is calculated, producing an error signal which is sent to the controller. To determine the optimal T_{set}, the T_{air} is adjusted within the system's setting range (18 °C to 30 °C), while keeping PMV determining variables of RH, V_{air}, I_{cl}, and M constant. During this process, the T_{mrt} is assumed to be equivalent to T_{air}. The selected new T_{set} is conveyed as a manipulated variable. An infrared (IR) sensor, acting as the actuator, sends the decided control set signal to the HVAC system installed indoors, executing the control for the next cycle.

2.3. Experimental information

2.3.1. Control target and participants

Experiments were conducted targeting both individual and multiple occupants. The experiment involving a single occupant was conducted to assess the efficacy of real-time PMV-based control, taking into account the changes in personal factors. Following the initial investigation, the optimal control strategy was investigated to maximize thermal comfort for the largest number of occupants within a communal environment.

A total of 11 participants were recruited, with 8 individuals conducting the single-occupant experiment and 3 participating in the

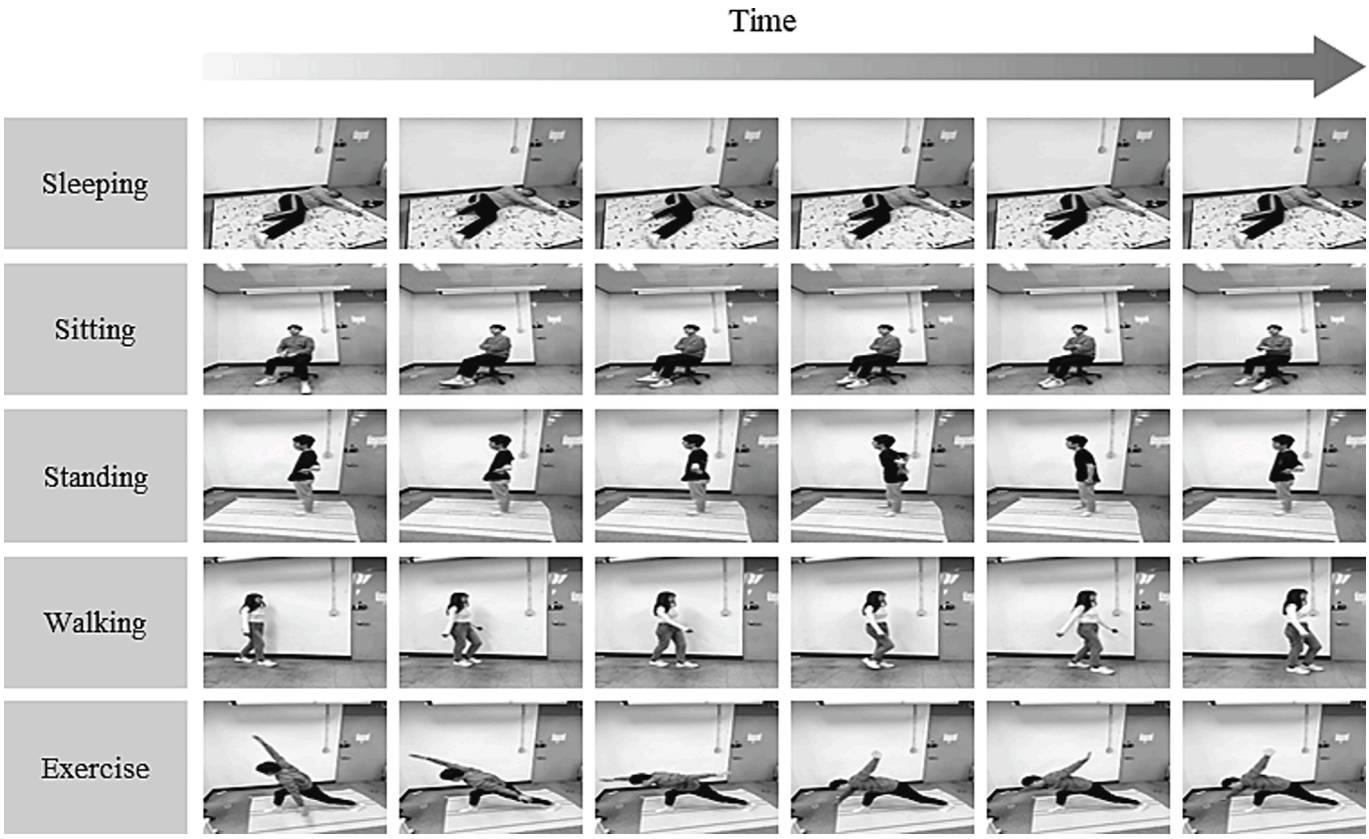

Fig. 2. Examples of consecutive image in training dataset.

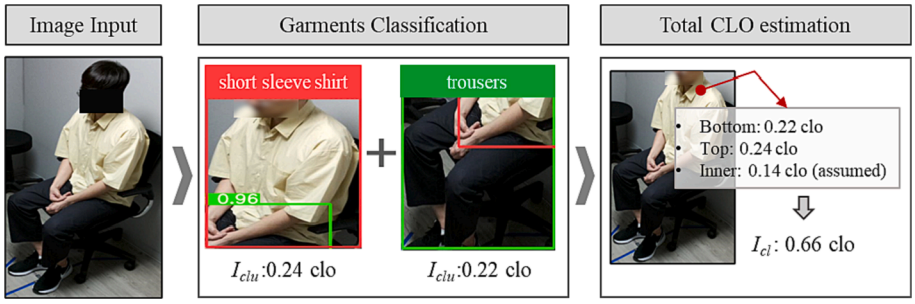

Fig. 3. Estimating process of CLO subnet.

Table 2
Types of garments.

Category	Label	Garment	I_{clu} [clo]
Top	G1	short sleeve shirt	0.24
	G2	long sleeve shirt	0.33
	G3	T shirt	0.10
	G4	long sleeve sweater	0.36
	G5	long sleeve sweatshirt	0.16
Bottom	G6	trousers (straight, loose)	0.22
	G7	knee length skirt	0.14
	G8	ankle length skirt	0.23
	G9	walking shorts	0.08
	G10	sweat pants	0.28
Outer	G11	suit jacket	0.36
Dress	G12	short sleeve shirt dress	0.29
	G13	long sleeve shirt dress	0.35
Pajama	G14	long sleeve pajama top	0.31
	G15	short sleeve pajama top	0.25
	G16	pajama trousers	0.17

multiple-occupant experiment. To minimize the potential effects attributed to the Body Mass Index (BMI) of the participants, the inclusion criteria were limited to those within the normal BMI range (18.5 kg/m^2 ≤ BMI < 25 kg/m^2). The participants had an average age of 26.9 years and an average BMI of 21.2 kg/m^2. During the experiment, subjective thermal sensations of the s were collected through surveys. The Thermal Sensation Vote (TSV) metric from ASHRAE standard 55 was employed for thermal sensation polling. This was assessed as an average value from continuous short-term votes, referred to as the point-in-time survey. Throughout the experiment, participants cast their votes at 2-min intervals. Due to missed votes and internet connectivity issues, there were slight discrepancies in the total number of votes.

2.3.2. *Control methods*

To assess the effectiveness of a thermal environment control strategy grounded in real-time PMV values, two additional control systems conventionally employed in the field were introduced for comparative analysis. Thus, a comparative evaluation was conducted across three distinct feedback control systems.

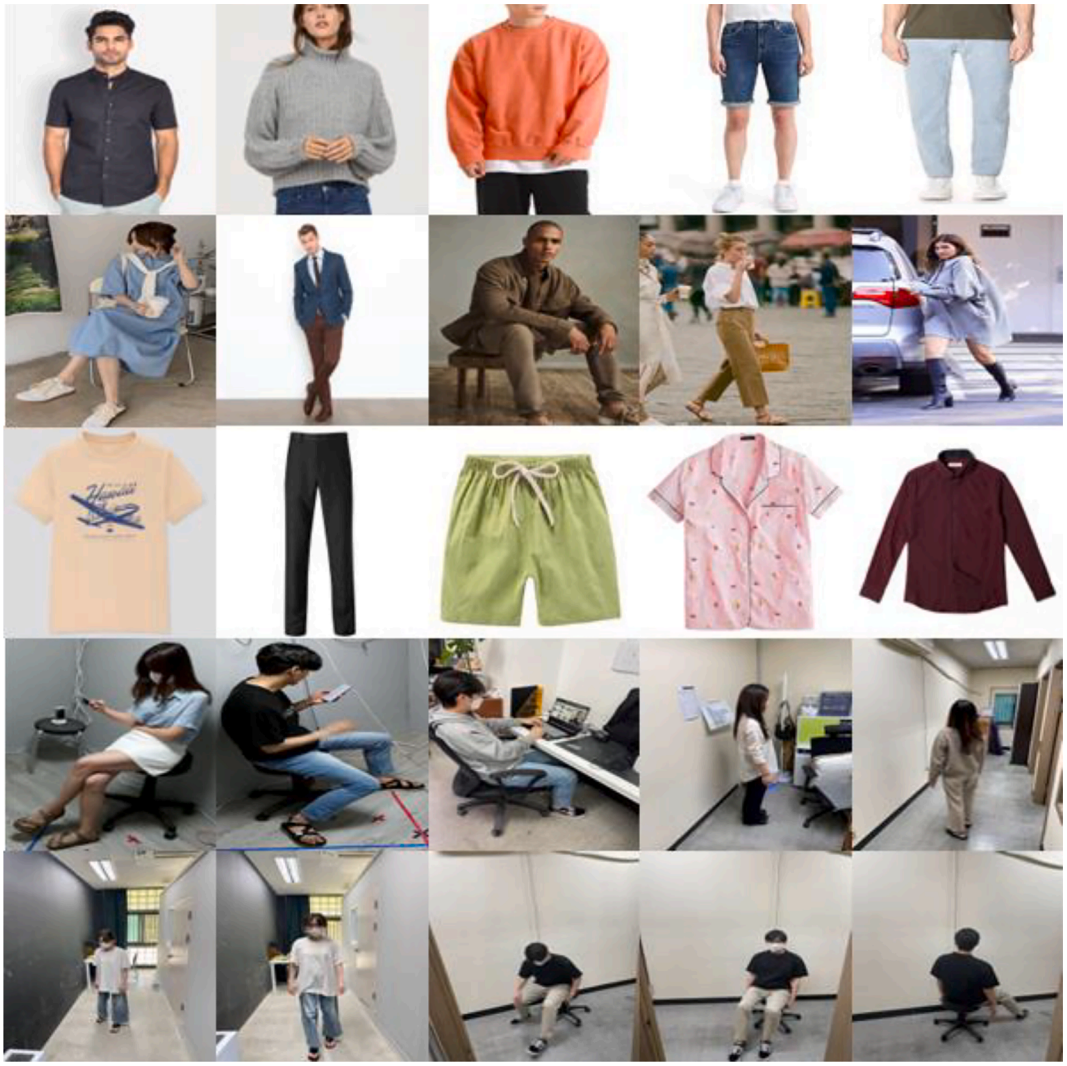

Fig. 4. Training dataset examples for CLO subnet.

The first system sets the air temperature as a control variable, referred to as the T_{air}-based control system (Base control system 1). The second system, the PMV-based control system without using the PF model (Base control system 2), calculates the PMV by employing fixed M and I_{cl} values, while the other four environmental variables (T_{air}, RH, T_{mrt}, V_{air}) are measured via sensors. For M, a value representing sedentary behavior, 1.0 met, was used. For I_{cl}, a value of 1.0 clo for the heating period was applied. The real-time PMV-based control system proposed in this study (Proposed control system) uses the PF model to consider both environmental and personal factors, employing the actual PMV as the control variable. For convenience, considering the characteristics of the three described control systems, they are named in this paper as follows:

- Base control system 1: T_{air}-based control
- Base control system 2: PMV_{fix}-based control
- Proposed control system: PMV_{real}-based control

The experiments were carried out in the heating season. Adhering to the guidelines from ASHRAE Standard 55, the indoor temperature setpoint was designated at 22 °C for the heating phase [11], while the PMV setpoint was established within a comfort threshold of −0.25. Typically, when setting indoor temperatures, considerations of energy efficiency and human thermal adaptability dictate the demarcation of separate set temperature ranges for heating and cooling. Analogously, PMV setpoints were differentiated based on periods, and for the heating period, a mid-range value of −0.25 was chosen, falling between −0.5 and 0.0 [39]. Each experiment was conducted for a duration of 30 min per cases of the occupant activity and clothing combination, transmitting control signals at 10-min intervals. Importantly, to minimize the impact of thermal sensations induced by consecutive activities on the participants, a rest period of 15 min was provided between experiments. Activities were conducted in a randomized order. Initial TSV data spanning the first 10 min were excluded from the analysis to account for participants' adaptation to the indoor environment.

2.3.3. Chamber information

For the experimental setup, a Test-bed measuring 5.4 m × 2.0 m × 2.2 m was constructed inside a building located in Seoul, South Korea (See Fig. 7). The atmospheric pressure at the location of the Test-bed is 1 atm. To facilitate the thermal environment control, a wall-mounted packaged terminal heat-pump air conditioning (AC) unit was installed. The cooling and heating capacities of this system are rated at 2.80 kW and 3.50 kW respectively, with a coefficient of performance (COP) of 3.64 for cooling and 3.89 for heating.

Within the Test-bed, various sensors, compatible with real-time data collection and communication platforms such as Arduino and Raspberry Pi, were deployed to measure environmental variables. Environmental sensors, capturing data for variables (T_{air}, RH, T_{mrt}, and V_{air}) were systematically positioned at a height of 1.2 m. Camera sensors were placed

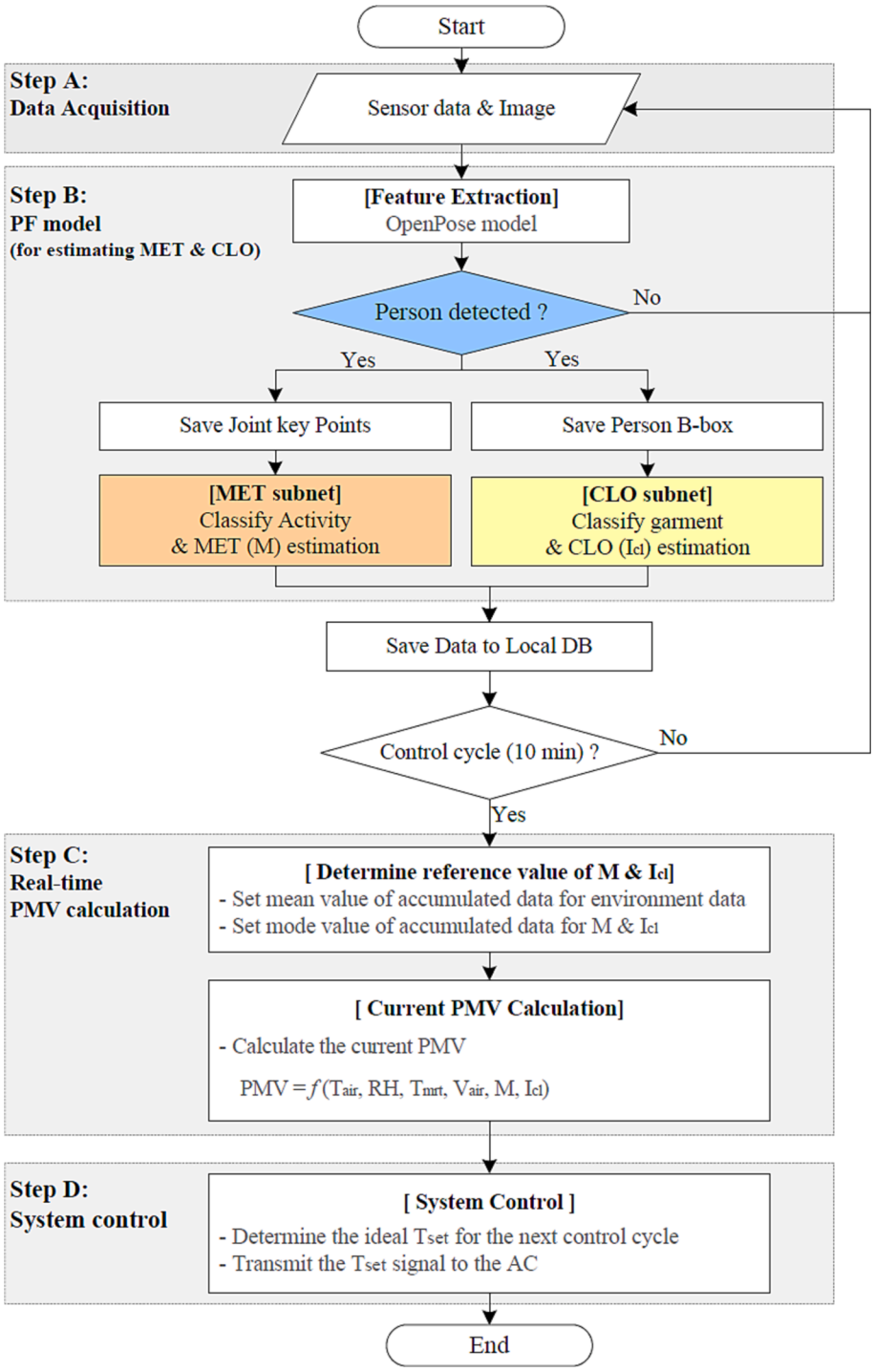

Fig. 5. Control algorithm employing the PF model.

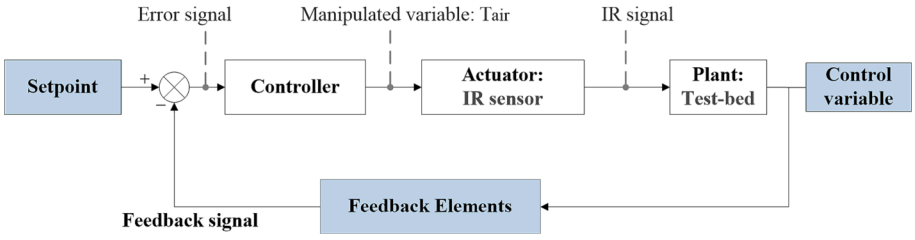

Fig. 6. Feedback control logic.

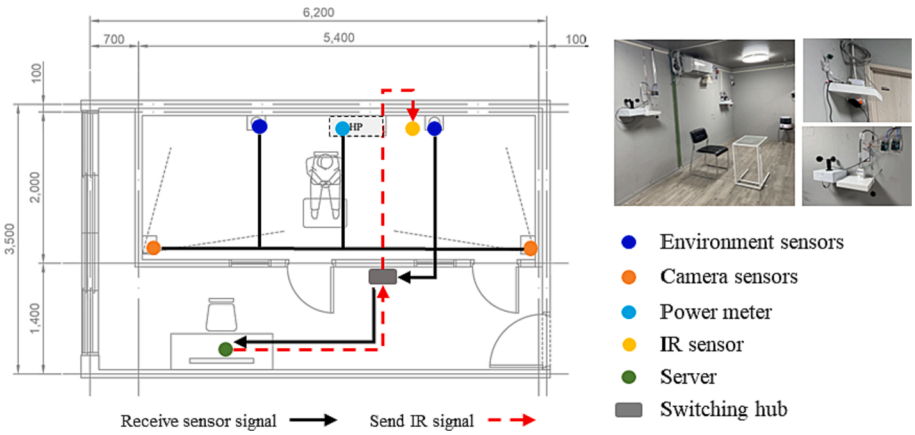

Fig. 7. Configuration of Test-bed.

at a height of 1.8 m on both sides of the interior to allow dual-angle data acquisition. In addition, a current sensor, designed to monitor the energy consumption of the AC system, and an IR sensor, used to transmit temperature control signals, were located in proximity to the AC unit. The data acquisition frequency for the environmental and current sensors was set at intervals of 15 s. While the camera system is capable of capturing up to 30 frames per second (FPS), considering the processing speed of the vision model and potential server load, images were stored at a rate not exceeding 2 FPS in this study.

2.3.4. Experimental conditions

The cases of M and I_{cl} combination, which the model can estimate, were predefined. Among the indoor activities that can be categorized under the MET subnet, three typical actions observed in residential and office settings were chosen: sitting (1.0 met), standing (1.2 met), and walking (1.7 met). For clothing, based on the 16 individual clothing items that the model can differentiate, three representative indoor clothing ensembles, typically worn as per ISO 9920 [40], were established: 0.50 clo, 0.74 clo, and 1.04 clo. The basic apparel including underwear, socks, shoes, and inner garments were consistently worn across the sets.

Within the Test-bed, furnishings were equipped to facilitate indoor activities, including chairs and a walking pad. The chairs selected for the experiment were of a standard type that doesn't require insulation value adjustments, ensuring they wouldn't influence the I_{cl} values [11]. Furthermore, during the experiments, participants were restricted from factors that could influence their thermal perception, such as wearing masks or consuming food and beverages. For experiments with a single occupant, a total of 9 experimental cases were conducted, with each case consisting of unique combinations of M and I_{cl} as detailed in Table 3.

In this study, the developed model was initially evaluated in a small-scale environment. Considering the dimensions of the test-bed, the experiments in the multiple-occupancy environment were conducted with a reference to 3 individuals. This serves as a step towards expanding the scale of occupants and laying the groundwork for practical, real-world experiments. From the individual variable cases delineated in Table 3, conditions for Case 1, 5, and 9 were designated, leading to a total of four cases as outlined in Table 4. Each case reflects the conditions for individual participants (p1-3), with two participants were set as undergoing identical conditions within the indoor environment.

Table 3
Experiment cases for a single subject.

Case	M [met]	I_{cl} [clo]
Case 1	1.0	0.50
Case 2	1.2	0.50
Case 3	1.7	0.50
Case 4	1.0	0.74
Case 5	1.2	0.74
Case 6	1.7	0.74
Case 7	1.0	1.04
Case 8	1.2	1.04
Case 9	1.7	1.04

3. Model performance for estimating personal factors

In this section, the performance of the PF model in determining personal factors is examined. The training outcomes of the PF model's each subnet was analyzed (section 3.1), and the accuracy when the two personal factors are derived in real-time within an experimental environment is assessed (section 3.2). Through this evaluation, the reliability of the model when employed in thermal environment control is intended to be validated.

3.1. Training results

The subnets that constitute the PF model were trained on the assembled RGB image dataset, classifying 5 activities and 16 individual clothing items, respectively. During training, the constructed dataset was divided into train, valid, and test datasets. The train and valid datasets were utilized for model training and validation, while the test dataset, consisting of data not used during training, was employed to evaluate model performance. Each model was trained to classify activities and attire from images, as explained in sections 2.1.1 and 2.1.2. Key classification model performance indicators for evaluating the trained models included the convergence of the loss function, confusion matrix, and F1 score, were utilized to evaluate the MET and CLO subnet.

The confusion matrix visualizes the model's classification performance for each class by displaying the results of actual and estimated data (Fig. 8). In this context, the true and false outcomes of the estimations are distinguished. True Positive (TP) and True Negative (TN) denote accurate predictions, while False Positive (FP) and False Negative (FN) indicate instances of misclassification. This matrix provides crucial metrics, including accuracy, precision, and recall. "Accuracy" represents the overall correctness of the model, "precision" denotes the

Table 4
Experiment conditions for multiple subject.

Multi-case	Person		
	P1	P2	P3
Multi-case 1	Case 1	Case 1	Case 5
Multi-case 2	Case 1	Case 1	Case 9
Multi-case 3	Case 5	Case 5	Case 1
Multi-case 4	Case 9	Case 5	Case 5

		Estimated		
		Positive	Negative	Index
Actual	Positive	True Positive (TP)	False Negative (FN)	Recall $\frac{TP}{TP+FN}$
	Negative	False Positive (FP)	True Negative (TN)	
	Index	Precision $\frac{TP}{TP+FP}$		Accuracy $\frac{TP+TN}{TP+FP+TN+FN}$

Fig. 8. Performance metrics of confusion matrix.

predictive accuracy of a specific class, and "recall" signifies the model's capability to detect all instances of a class. The main diagonal of the confusion matrix depicts classification accuracy, and the F1 score, computed according to Eq. (2). F1 score represents the harmonic mean of precision and recall; a score closer to 1 indicates superior model performance.

$$F1score = \frac{2 \times Precision \times Recall}{Precision + Recall} \tag{2}$$

3.1.1. Training results of MET subnet

The MET subnet, based on DNN, conducted performance evaluation concerning the number of hidden layers and neurons. Experiments were conducted with three hidden layers and neuron counts ranging from 10 to 50. The optimal model performance entails the loss value converging to 0 as the training epochs increase. Fig. 9(a) depicts the loss function across the five network structures. As evident from the figure, the optimal structure was identified with three hidden layers and 50 neurons. Any neuron count exceeding 50 did not substantially contribute to accuracy enhancement and led to issues of overfitting and performance degradation.

The optimal MET subnet's confusion matrix result for the test dataset is as depicted in Fig. 9(b). It displayed an average classification accuracy of 0.95, with F1 scores averaging 0.97, which is proximate to 1. Upon analyzing each class, the activity with the lowest accuracy was "walking," primarily misclassified as "standing." This suggests that momentarily captured images of walking postures can sometimes resemble standing postures, leading to such misclassification errors.

3.1.2. Training results of CLO subnet

The CLO subnet was trained using a batch size of 16 and for 150 epochs [28]. Various data augmentation techniques were implemented to enhance robustness and prevent overfitting. Examples of these techniques include image resizing, random cropping, mirroring, angular rotation, HSV transformation, and mosaic. The training outcome of the CLO subnet is illustrated in Fig. 10(a), where the error graph differentiates between the detecting loss and classification loss for clothing. Detecting loss signifies the error in detecting clothing within images, while classification loss represents the error in classifying the detected clothing. Both errors demonstrated a convergence to 0. The confusion matrix for the CLO subnet concerning the test dataset is presented in Fig. 10(b), showing an average accuracy of approximately 0.95 across all classes. Excluding two clothing types, the accuracy consistently exceeded 0.9. Upon examining the F1 score, an average score of 0.93 was observed for all classes.

3.2. Performance assessment in lab environment for model validation

To validate the performance and reliability of the model, preliminary

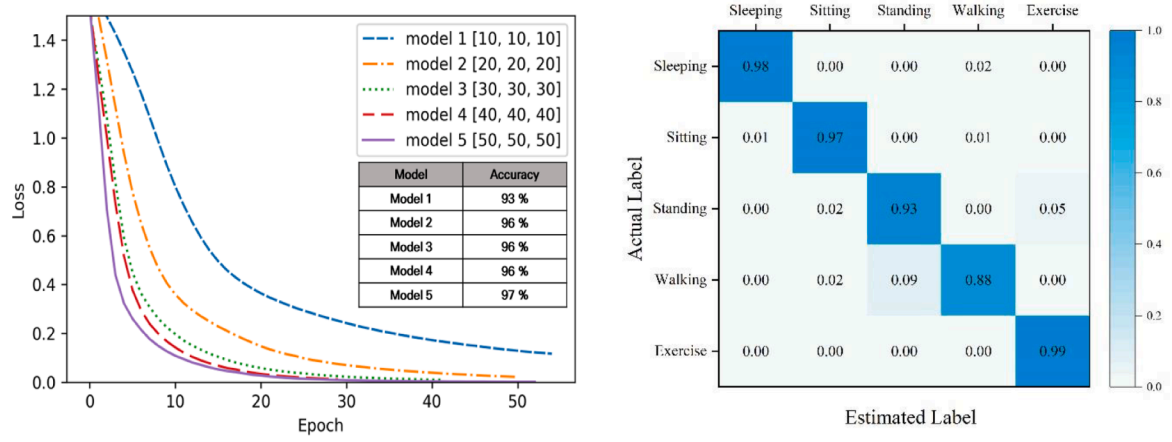

(a) (b)

Fig. 9. MET subnet training results: a) Loss function results and b) Confusion matrix result of the test dataset.

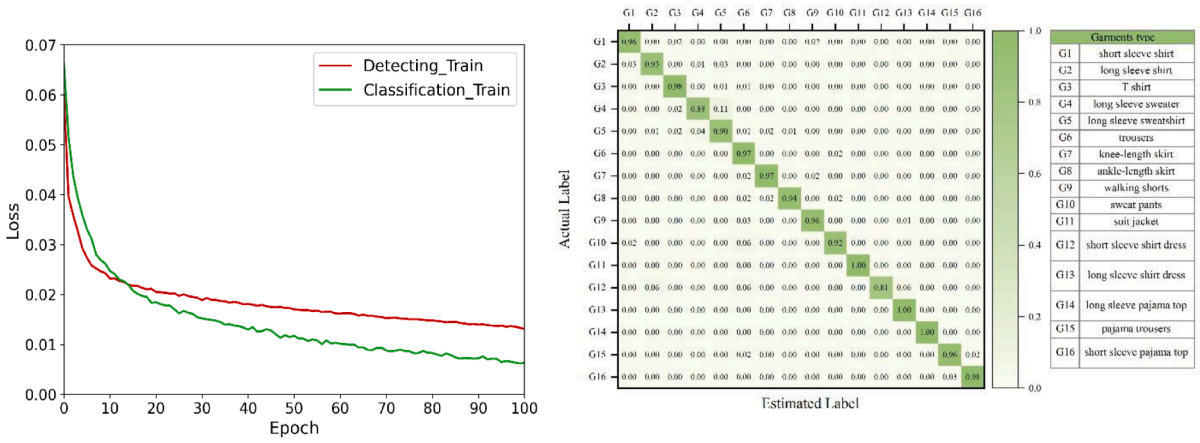

(a) (b)

Fig. 10. CLO subnet training results: a) Loss function results and b) Confusion matrix result of the test dataset.

tests were conducted in an actual lab environment using untrained data. Based on the activity and clothing combinations of Table 3, tests were executed at 5-min intervals across 9 cases. The accuracy of the two personal factors was assessed using representative values from both 1 min and 5 min data. These representative values were determined by the mode data within the given duration: 60 data points for 1 min and 300 data points for 5 min.

Fig. 11 presents the model's performance of representative values. Fig. 11(a) displays the M and I_{cl} representative values based on a 1-min duration. The mean absolute error (MAE) for M was 0.04 met, primarily arising from the Standing (1.2 met) posture. This can be attributed to changes in joint coordinates when a person shifts their position while standing. The MAE for I_{cl} was 0.03 clo, primarily resulting from clothing being obscured due to pose changes.

Fig. 11(b) illustrates the mode data over 5 min using bar graphs. The mode values of M and I_{cl} for all cases matched the actual values. By employing accumulated data for more than 5 min, transient classification errors and outliers can be minimized, enhancing the accuracy of individual variable derivation. Consequently, this study adopted a 10-min control cycle aiming to improve the precision of the thermal environment control system.

4. Thermal control results based on the real-time PMV

In this section, the effectiveness of the proposed control system was analyzed. The thermal control effects for a single individual were assessed, and the feasibility of PMV-based control in ensuring thermal comfort for multiple occupants was verified. The experiments were conducted between January and February, during which the average outdoor temperature was 0.49 ℃, and the average humidity was 60.9 %, indicative of a heating period.

4.1. Assessment in the single-person environment

4.1.1. Results of thermal environment and thermal comfort

The participants executed the 9 case conditions from Table 3 for 30 min each in the Test-bed. Three control methods were applied randomly; Tair-based control set the temperature to 22 ℃, while for the PMV-based control, the PMV setpoint was set at −0.25. Before analyzing the control results, the accuracy of the M and I_{cl} values as derived by the PF model was first confirmed. Based on the MAE of the model, MET subnet had a maximum error of 0.031 met and CLO subnet showed a maximum error of 0.028 clo, both indicating low error values. The accuracy was consistent regardless of the camera's angle, suggesting that real-time control was appropriately executed. Examples of the MET and CLO subnet results during control are depicted in Fig. 12.

The indoor T_{set} varied depending on the control system (Fig. 13). Unlike other control system, the PMV_{real}-based control determined the T_{set} over a broad range from 19℃ to 27℃, taking into account variations in personal factors. For Case 1 and Case 2, which had lower M and I_{cl} values, a relatively higher indoor temperature was established. Conversely, in Case 8 and Case 9, where both M and I_{cl} were higher, a cooler indoor environment was set.

During all experimental conditions, the RH was consistently stabilized at approximately 30 %. Owing to the air turbulence induced by the heating system's operation, the V_{air} registered an average value of 0.08 m/s. The T_{mrt} was typically observed to be around 0.6 ℃ lower than the ambient indoor temperature. Leveraging the gathered environmental parameters and personal factors, the PMV was calculated for each respective control system. The outcomes are systematically presented in Fig. 14: Fig. 14(a) delineates the data point distribution across control systems, while Fig. 14(b) employs a box plot to provide a portrayal of the PMV distribution for individual cases.

Based on Fig. 14(a), the PMV_{real}-based control exhibited the highest comfort level, accounting for 82.8 % of all data points within the comfort range, outperforming PMV_{fix}-based control (53.4 %) and T_{air}-based control (49.2 %). This emphasizes the superior efficiency of the proposed PMV_{real}-based system in achieving optimal comfort.

Fig. 14(b) reveals a significant PMV variance between Case 1 (with the minimal M and I_{cl}) and Case 9 (with the maximal M and I_{cl}): 2.3 for the T_{air}-based system and 1.9 for the PMV_{fix}-based system, highlighting the inherent discrepancies between control methodologies. Contrarily, the proposed method manifested a minimal PMV deviation of 0.9, consistently maintaining values closest to PMV 0, among the three of control strategies. Especially in instances where M and I_{cl} values are exceptionally low or high (as in Case 1 and Case 9), there's a noticeable improvement in thermal comfort compared to base control systems. Across the board, the proposed system's PMV spanned from −0.67 to + 0.29. With a designated PMV setpoint at −0.25, the indoor temperature deadband was reduced, leading to the appearance of some data points below −0.5.

Based on the PMV results, the actual thermal comfort outcomes as indicated by TSV were also analyzed. The experimental dataset encompassed around 2,160 TSV observations, visualized as a box plot in Fig. 15, with the delineation of the comfort zone. For the PMV_{real}-based control system, the average TSV for all cases was within ± 0.2, satisfying the comfort range. Notably, with the sole exception of Case 9, the TSV data predominantly clustered around zero. Conversely, for the

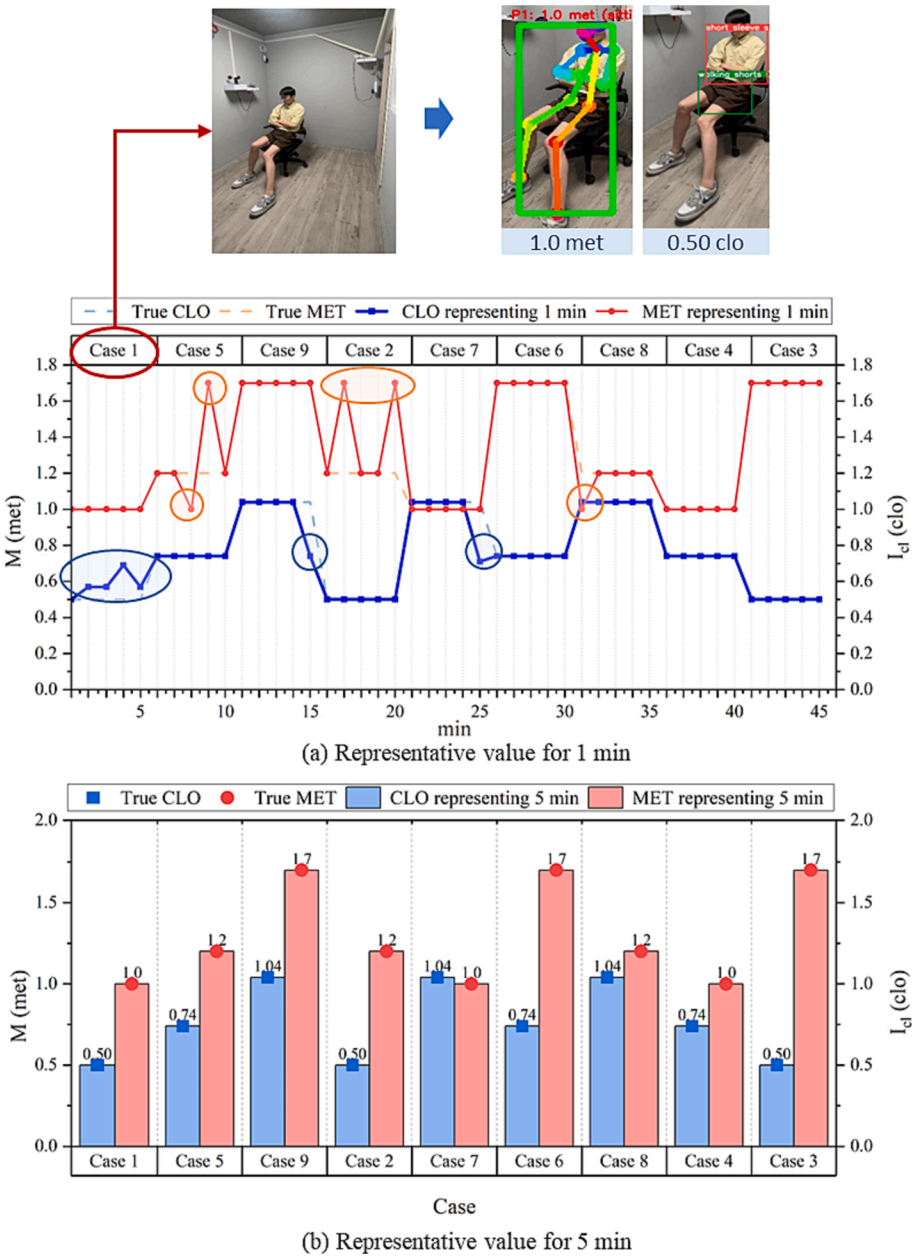

Fig. 11. Model performance by applying in the real environment.

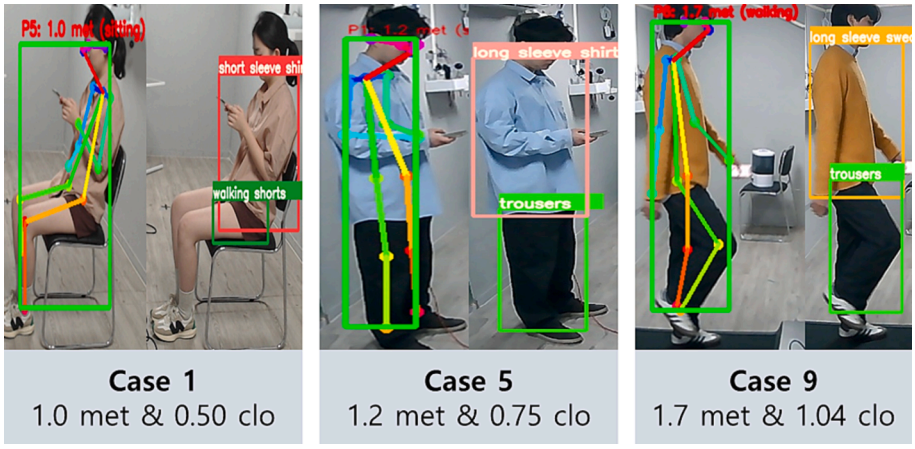

Fig. 12. Example results of personal factors estimation.

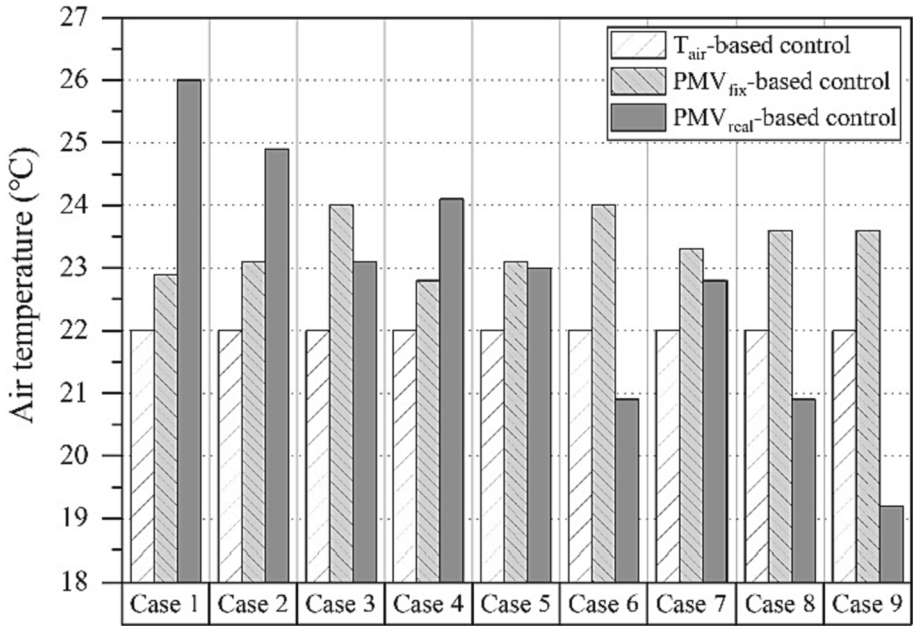

Fig. 13. Indoor T_{set} by control methods.

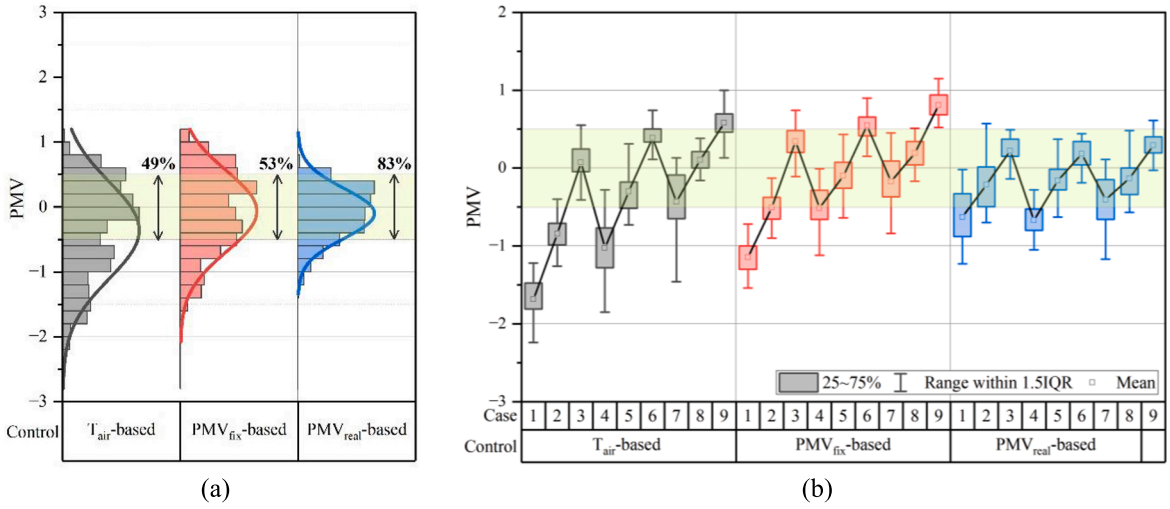

Fig. 14. PMV distribution results: a) Results by control system and b) Results by case.

alternative control systems, certain scenarios manifested TSV distributions and mean values deviating from the comfort range, signifying potential discomfort for the occupants.

In assessing the total TSV data points, the PMV_{real} -based control exhibited the highest comfort range inclusion at 73.2 %, followed by the PMVfix-based control at 59.9 %, and lastly the Tair-based control at 57.3 %. This hierarchy parallels the findings from the PMV control. The PMV_{real}-based control system registered a notable 13.3 % increase in thermal comfort relative to its counterparts. Moreover, a significant 97.8 % of the data converged within the −1 to + 1 interval, predominantly manifesting during periods of indoor temperature transitions.

In summary, the proposed PMV_{real}-based control system consistently outperforms conventional methodologies in ensuring a comfortable thermal environment. It's particularly noteworthy that, with a PMV setpoint of −0.25, a majority of participants experienced optimal thermal comfort, affirming the efficacy of this setting throughout the heating season.

4.1.2. *Energy consumption results*

In this section, the heating energy consumption associated with each control method was examined. Energy consumption was assessed by measuring the AC system's power usage throughout the 30 min experimental period. The initial 10 min of data were excluded from all analyses to account for participants' adaptation periods to the indoor environment. As a result, Fig. 16 illustrates the average energy consumption per case for all participants, presented as energy consumption per unit area (kJ/m^2). The disparities in energy consumption between the proposed control system and the other two control approaches are delineated in a table beneath the figure.

Upon reviewing Fig. 16, the energy consumption of the heating system, intended to elevate the indoor temperature, closely mirrors the trends observed in the indoor temperature graphs. The PMV_{real}-based control system showcased a varied energy consumption, spanning from 131.9 kJ/m^2 to 362.1 kJ/m^2 across different cases. Notably, as the M value transitioned from 1.0 met to 1.7 met across the cases (specifically from Case 1 → 3, 4 → 6, and 7 → 9), there was a discernible 43 %

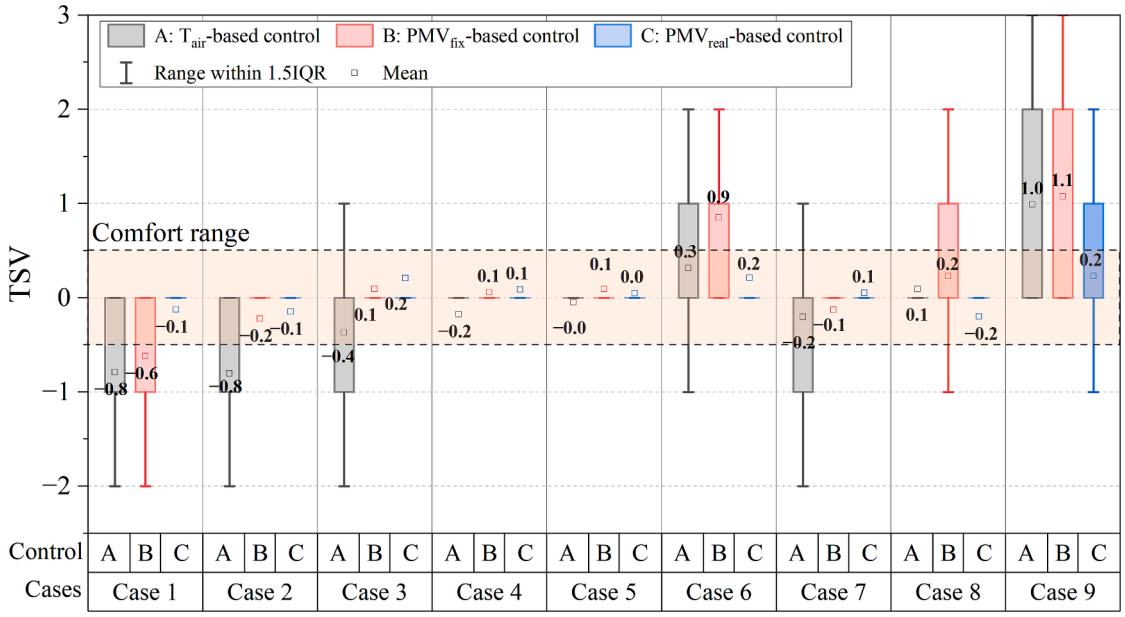

Fig. 15. TSV distribution results.

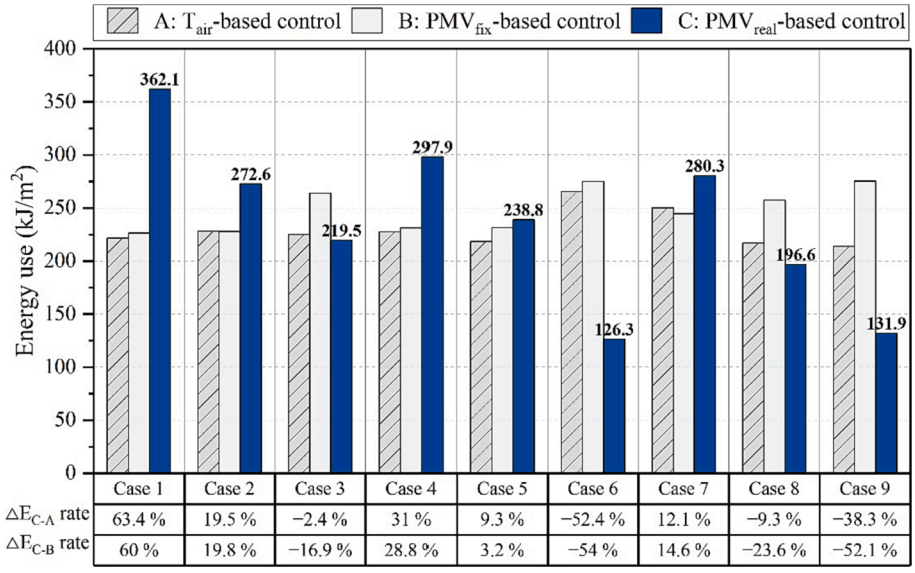

Fig. 16. Average heating energy by control systems.

reduction in energy consumption. In contrast, a shift in the I_{cl} value from 0.50 clo to 1.04 clo (observed from Case 1 → 7, 2 → 8, and 3 → 9) resulted in a 22 % decline in energy usage. The reduced energy consumption in Case 6, relative to Case 9, can be attributed to occasional higher external temperatures, which in turn augmented the efficiency of the heat pump.

In scenarios like Case 1, where both personal factors were at their minimums, energy consumption surged by up to 63.4 %. However, as these factors increased, seen in Cases 6 and 9, energy consumption demonstrated potential reductions of up to 54 % compared to conventional control approaches. Although the proposed methodology might not consistently outperform in all energy efficiency contexts, it indicates that when aptly applied in specific conditions, substantial energy efficiency gains can be realized.

To further optimize energy efficiency, a comprehensive thermal environment control should be considered. This approach would not only focus on indoor temperature but also incorporate other impactful PMV variables such as RH, T_{mrt}, and V_{air}. Additionally, the integration of supplementary systems, like the personal comfort systems (PCS), may further bolster energy conservation strategies.

4.2. Assessment in the multi-occupant environment

In multi-occupant environments, determining an optimal PMV value to ensure collective comfort is paramount. Notably, relying solely on average PMV values for a group can lead to considerable variations in individual thermal sensations, as indicated by previous studies [6,41]. In this research, the potential benefits of using the most frequently derived personal factors for the group are sought to be evaluated, contrasting its effectiveness with an approach based on average values.

4.2.1. Estimation accuracy of the personal factors for multiple occupants

The precision of the PF model was assessed as a preliminary step using data from multiple participants. Based on the designated activity

and clothing conditions presented in Table 4, participants derived three M and I_{cl} values from one image frame. The representative M and I_{cl} values were ascertained using either the mode or mean value of the accumulated 10-min data. This section delves into an analysis of the error between the representative output value for the control duration and the actual observed data to evaluate the model's efficacy.

The analysis revealed that the mode-based method for determining M and I_{cl} values consistently yielded accurate outcomes across all multi-cases. Conversely, utilizing the mean of accumulated data introduced discrepancies, resulting in deviations of up to 0.14 met and 0.03 clo. Consequently, the mode-based approach exhibited superior precision in representing an occupant's M and I_{cl} values. Fig. 17 showcases examples of individual M and I_{cl} determinations for each multi-case.

4.2.2. Thermal control assessment with real-time PMV for multiple occupants

To determine the representative PMV, this study employed two methods to obtain a single value for M and I_{cl}, representing the overall space. One method involves utilizing the mode value, representing the most frequent value among three participants, while the other method involves using the mean value, which is the average of these three participant values. Both the mode and the mean of three participants' values were utilized to control the heating system. Subsequently, a comprehensive analysis was conducted, considering both indoor environmental factors and the thermal comfort of the occupants. Fig. 18 depicts the average control T_{set} for each method. When employing the mode, there was a significant variation in indoor temperature across cases compared to when using the mean.

In the constructed indoor environments based on different methodologies, the distribution of individual PMV and the mean TSV for the three participants are illustrated in Fig. 19. Specifically, Fig. 19(a) presents the results of the PMV_{real}-based control system leveraging mode values, while Fig. 19(b) exhibits the outcomes when utilizing mean values. The individual PMV distributions are based on the collected data, while the TSV reflects the participants' reported thermal sensations during the experiment.

The left-side graph of Fig. 19 provides an in-depth analysis of PMV outcomes. Here, the control method based on the mode values strategically emphasizes a broad set of individual parameters, successfully

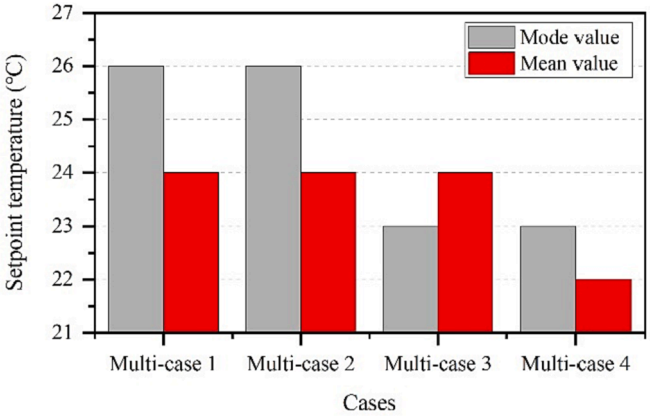

Fig. 18. Temperature setpoint by control method.

ensuring the thermal comfort for a minimum of two participants across all scenarios. However, the control strategy based on mean values demonstrated potential vulnerabilities, particularly in scenarios such as Multi-case 2. In such instances, notable disparities in occupants' M and I_{cl} might lead to a scenario where all participants' PMVs fall outside the accepted comfort zone.

The right-side graph displays the TSV analytical outcomes. Under the mode-based control approach, the majority of scenarios exhibited thermal sensations within the comfort spectrum. Nevertheless, for P3 in Multi-case 2 of Fig. 19(a), the TSV situated itself in the discomfort domain, presumably due to the combination of high indoor temperature and tight clothing leading to sweating and increased discomfort. Conversely, as depicted in Fig. 19(b), using the mean value steered certain scenarios, specifically Case 1 and Case 2, away from the defined comfort bounds. In particular, during Multi-case 2, the three participants reported different TSV, suggesting a potentially lower level of comfort for the majority of occupants.

In conclusion, employing the mode of individual variables emerges as a preferable strategy to optimize thermal comfort for the largest number of occupants. Yet, this approach is not devoid of its limitations, especially evident in situations like Multi-case 2, while a majority might

Fig. 17. Examples of M and I_{cl} estimation in multi-occupants cases.

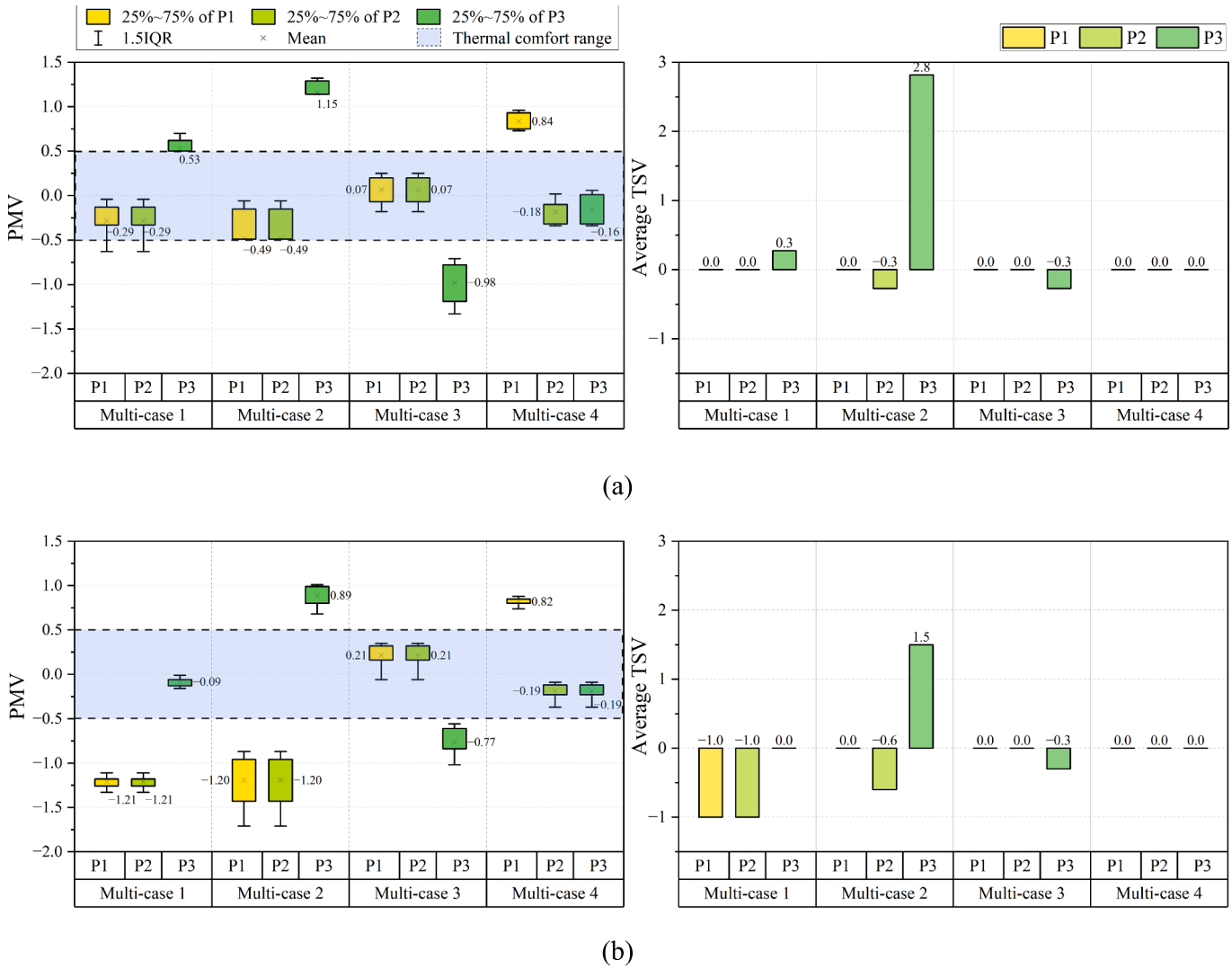

Fig. 19. Thermal comfort results in the multi occupant settings: a) Mode value results and b) Mean value results.

find the environment pleasant, certain occupants could still experience notably adverse conditions. This implies that when addressing groups, there exists a need to augment individual thermal environments, potentially through ancillary systems tailored for those few who perceive disparate thermal sensations.

5. Discussion

In this research, an intelligent vision-based model was effectively employed to estimate individual M and I_{cl} values. The model has proven adept at accommodating a wide range of daily activities and clothing choices, showing its potential for environments with multiple occupants. The developed PF model necessitates continual enhancement through the construction of extensive datasets. Specifically, the integration with other vision models, such as object recognition systems, is anticipated to aid in classifying diverse activities and clothing. Concurrently, issues related to personal data protection must be critically addressed [42–44]. It is worth considering the adoption of measures such as data anonymization, which removes identifiable details, or data obfuscation that introduces noise to prevent personal identification, thereby ensuring heightened data security.

Through the implementation of real-time PMV-based control system, the potential for enhancing occupants' thermal comfort was identified. These findings provide empirical support for the efficacy of prior research [23,28]. Nevertheless, relying solely on a single heating and cooling system poses challenges in ensuring thermal comfort for all occupants. In response, the integration of auxiliary systems, such as the PCS, could be contemplated. Furthermore, the expansion and incorporation of computer vision techniques to detect residents' discomfort offers potential for the development of personalized heating and cooling strategies.

Moreover, improvements in thermal comfort models, specifically those utilized as control variables, are imperative for the accurate evaluation of thermal comfort. Given that the developed PF model facilitates the estimation of personal factors influencing an individual's thermal sensation, there is an opportunity to employ these variables as a foundation to a novel thermal comfort model. Furthermore, a refined thermal comfort model can be formulated, integrating supplementary individual variables, including gender and BMI, to enchance the precision of regulating the thermal environment.

This study is grounded in experiments with a restricted set of participants and settings. As a result, broader validation through Living Lab assessments in diverse contexts and larger participant groups is essential. Notably, understanding seasonal variations in thermal perception and control strategies necessitates additional trials during cooling periods. Regarding energy consumption, a comprehensive examination of energy patterns for comfort-centric controls across various building types and HVAC systems is essential to enhance the efficiency of

building operations. With sustained research and refinements, the thermal environment control strategy proposed here is projected to achieve zone-specific, user-customized control in indoor spaces with multiple occupants.

6. Conclusion

In the presented study, a real-time PMV-based control method was developed that leverages the M and I_{cl} information of occupants. Utilizing this method, thermal environment control experiments were conducted on actual occupants, leading to an analysis of the influence of real-time occupant information on comfort and system energy consumption. Through the use of images, the developed PF model was shown to objectively estimate M and I_{cl} values in both individual and multiple occupant scenarios. By employing representative values from cumulative data, transient errors were reduced, and the precision in determining personal factors was enhanced. The indoor set temperature was adjusted by the real-time PMV-based control, resulting in a verified enhancement in occupant thermal comfort, marking a more than 13.3 % improvement in actual participant's thermal sensation compared to conventional control systems. Additionally, in environments with multiple occupants, it was ascertained that the effective approach to ensure comfort for the majority was to apply the mode values of M and I_{cl} from multiple participants. Ultimately, the efficacy of the suggested methodology in consistently delivering a comfortable thermal environment, irrespective of changes in an occupant's personal factors, was confirmed.

It is clearly established that comfort-oriented control system can lead to fluctuations in energy consumption based on the conditions of the occupants. Based on the findings of this research, there is potential to develop a monitoring and decision-support system, harmonizing both comfort and energy efficiency in response to occupants' dynamic conditions. Integrating with technologies such as IoT and smart home services, this can emerge as a pivotal solution for superior indoor thermal environment management. Leveraging such technology is expected to deliver a tailored comfort environment considering the occupants' situation, potentially enhancing their health, comfort, and productivity, thereby elevating overall wellbeing. Moreover, by integrating the developed model with other OCC control strategies that convey occupancy presence and patterns, it is expected that enhanced energy efficiency can be attained while ensuring achieving thermal comfort.

7. Declaration of Generative AI and AI-assisted technologies in the writing process

During the preparation of this work the authors used OpenAI's tool ChatGPT in order to improve readability and language. After using this tool, the authors carefully reviewed and edited the content as needed and take full responsibility for the content of the publication.

CRediT authorship contribution statement

Eun Ji Choi: Methodology, Software, Validation, Writing – original draft, Writing – review & editing. **Ji Young Yun:** Methodology, Visualization. **Young Jae Choi:** Methodology, Investigation, Data curation. **Min Chae Seo:** Investigation, Data curation. **Jin Woo Moon:** Conceptualization, Supervision, Project administration, Funding acquisition.

Declaration of competing interest

The authors declare that they have no known competing financial interests or personal relationships that could have appeared to influence the work reported in this paper.

Data availability

The data that has been used is confidential.

Acknowledgements

This work was supported by the National Research Foundation of Korea (NRF) grant funded by the Korea government (MSIT) (2019R1A2C1084145 and RS-2023-00217322) and Chung-Ang University Graduate Research Scholarship in 2022.

References

[1] S. Altomonte, S. Schiavon, M.G. Kent, G. Brager, Indoor environmental quality and occupant satisfaction in green-certified buildings, Build. Res. Inf. 47 (3) (2019) 255–274.
[2] K.W. Tham, H.C. Willem, Room air temperature affects occupants' physiology, perceptions and mental alertness, Build. Environ. 45 (1) (2010) 40–44.
[3] R. Widiastuti, J. Zaini, W. Caesarendra, Field measurement on the model of green facade systems and its effect to building indoor thermal comfort, Measurement 166 (2020) 108212.
[4] G.H. Merabet, M. Essaaidi, M. Ben Haddou, B. Qolomany, J. Qadir, M. Anan, A. Al-Fuqaha, M.R. Abid, D. Benhaddou, Intelligent building control systems for thermal comfort and energy-efficiency: A systematic review of artificial intelligence-assisted techniques, Renew. Sust. Energ. Rev. 144 (2021) 110969.
[5] J.Q. Xie, H.Y. Li, C.T. Li, J.S. Zhang, M.H. Luo, Review on occupant-centric thermal comfort sensing, predicting, and controlling, Energ. Build. 226 (2020) 110392.
[6] Z. Wang, R. de Dear, M.H. Luo, B.R. Lin, Y.D. He, A. Ghahramani, Y.X. Zhu, Individual difference in thermal comfort: A literature review, Build. Environ. 138 (2018) 181–193.
[7] C. Turhan, S. Simani, G.G. Akkurt, Development of a personalized thermal comfort driven controller for HVAC systems, Energy 237 (2021) 121568.
[8] P.O. Fanger, Thermal comfort. Analysis and applications in environmental engineering, Danish Technical Press, Copenhagen, 1970.
[9] C. Zhong, J.H. Choi, Development of a data-driven approach for human-based environmental control, Procedia Eng. 205 (2017) 1665–1671.
[10] F. Jazizadeh, A. Ghahramani, B. Becerik-Gerber, T. Kichkaylo, M. Orosz, Human-Building interaction framework for personalized thermal comfort-driven systems in office buildings, J. Comput. Civ. Eng. 28 (1) (2014) 2–16.
[11] ASHRAE Standard 55, Thermal Environmental Conditions for Human Occupancy, in, American Society of Heating, Refrigerating and Air-Conditioning Engineers, Atlanta, GA, USA, 2020.
[12] J.H. Choi, V. Loftness, Investigation of human body skin temperatures as a bio-signal to indicate overall thermal sensations, Build. Environ. 58 (2012) 258–269.
[13] M.H. Hasan, F. Alsaleem, M. Rafaie, Sensitivity study for the PMV thermal comfort model and the use of wearable devices biometric data for metabolic rate estimation, Build. Environ. 110 (2016) 173–183.
[14] S.C. Liu, S. Schiavon, H.P. Das, M. Jin, C.J. Spanos, Personal thermal comfort models with wearable sensors, Build. Environ. 162 (2019) 106281.
[15] D. Li, C.C. Menassa, V.R. Kamat, Personalized human comfort in indoor building environments under diverse conditioning modes, Build. Environ. 126 (2017) 304–317.
[16] H. Na, J.H. Choi, H. Kim, T. Kim, Development of a human metabolic rate prediction model based on the use of Kinect-camera generated visual data-driven approaches, Build. Environ. 160 (2019) 106216.
[17] S.R. Gao, Y.C. Zhai, L. Yang, H. Zhang, Y.F. Gao, Preferred temperature with standing and treadmill workstations, Build. Environ. 138 (2018) 63–73.
[18] K. Lee, H. Choi, J.H. Choi, T. Kim, Development of a data-driven predictive model of clothing thermal insulation estimation by using advanced computational approaches, Sustainability-Basel 11 (20) (2019).
[19] E.J. Choi, Y. Yoo, B.R. Park, Y.J. Choi, J.W. Moon, Development of occupant pose classification model using deep neural network for personalized thermal conditioning, Energies 13 (1) (2020).
[20] E.J. Choi, J.W. Moon, J.H. Han, Y. Yoo, Development of a deep neural network model for estimating joint location of occupant indoor activities for providing thermal comfort, Energies 14 (3) (2021).
[21] J.S. Liu, I.W. Foged, T.B. Moeslund, Automatic estimation of clothing insulation rate and metabolic rate for dynamic thermal comfort assessment, Pattern Anal. Appl. 25 (3) (2022) 619–634.
[22] J.S. Liu, I.W. Foged, T.B. Moeslund, Clothing insulation rate and metabolic rate estimation for individual thermal comfort assessment in real life, Sensors-Basel 22 (2) (2022).
[23] H. Choi, B. Jeong, J. Lee, H. Na, K. Kang, T. Kim, Deep-vision-based metabolic rate and clothing insulation estimation for occupant-centric control, Build. Environ. 221 (2022) 109345.
[24] J.H. Lee, Y.K. Kim, K.S. Kim, S. Kim, Estimating clothing thermal insulation using an infrared camera, Sensors-Basel 16 (3) (2016).
[25] K. Lee, H. Choi, H. Kim, D.D. Kim, T. Kim, Assessment of a real-time prediction method for high clothing thermal insulation using a thermoregulation model and an infrared camera, Atmosphere-Basel 11 (1) (2020).

[26] H. Choi, H. Na, T. Kim, T. Kim, Vision-based estimation of clothing insulation for building control: a case study of residential buildings, Build. Environ. 202 (2021) 108036.
[27] E.J. Choi, B.R. Park, N.H. Kim, J.W. Moon, Effects of thermal comfort-driven control based on real-time clothing insulation estimated using an image-processing model, Build. Environ. 223 (2022) 109438.
[28] E.J. Choi, Y.J. Choi, N.H. Kim, J.W. Moon, Seasonal effects of thermal comfort control considering real-time clothing insulation with vision-based model, Build. Environ. 235 (2023) 110255.
[29] H. Matsumoto, Y. Iwai, H. Ishiguro, Estimation of Thermal Comfort by Measuring Clo Value without Contact, in: In MVA, 2011, pp. 4.
[30] H. Choi, C.Y. Um, K. Kang, H. Kim, T. Kim, Review of vision-based occupant information sensing systems for occupant-centric control, Build. Environ. 203 (2021) 108064.
[31] W. O'Brien, A. Wagner, M. Schweiker, A. Mahdavi, J. Day, M.B. Kjaergaard, S. Carlucci, B. Dong, F. Tahmasebi, D. Yan, T.Z. Hong, H.B. Gunay, Z. Nagy, C. Miller, C. Berger, Introducing IEA EBC annex 79: Key challenges and opportunities in the field of occupant -centric building design and operation, Build. Environ. 178 (2020).
[32] Z. Cao, T. Simon, S.E. Wei, Y. Sheikh, Realtime Multi-Person 2D Pose Estimation using Part Affinity Fields, Proc. CVPR IEEE (2017) 1302–1310.
[33] A. Toshev, C. Szegedy, DeepPose: Human Pose Estimation via Deep Neural Networks, 2014 IEEE Conference on Computer Vision and Pattern Recognition (CVPR), (2014) 1653–1660.
[34] A. Kendall, M. Grimes, R. Cipolla, PoseNet: A Convolutional Network for Real-Time 6-DOF Camera Relocalization, IEEE I Conf. Comp. Vis. (2015) 2938–2946.
[35] G. Jocher, K. Nishimura, T. Mineeva, R. Vilarino, YOLOv5, https://ultralytics.com/yolov5, in, 2020.05.
[36] B.R. Park, E.J. Choi, Y.J. Choi, J.W. Moon, Accuracy analysis of DNN-based pose-categorization model and activity-decision algorithm, Energies 13 (4) (2020).
[37] F. Chen, Q. Zhao, Realtime action recognition, https://github.com/felixchenfy/Realtime-Action-Recognition, in, github, 2021.
[38] E.J. Choi, Building Thermal Control based on Real-time Metabolic Rate and Clothing Insulation of Occupants by Image data, Chung-Ang University, 2023.
[39] J.W. Moon, ANN-Based Model-Free Thermal Controls for Residential Buildings, University of Michigan, 2009.
[40] ISO 9920:2007, Ergonomics of the thermal environment — Estimation of thermal insulation and water vapour resistance of a clothing ensemble, in, ISO, Switzerland: International Organization for Standardization, 2007.
[41] E.A. McCullough, A Data Base or Determining the Evaporative Resistance of clothing, ASHRAE Trans. 91 (1989) 18.
[42] H. Hukkelas, R. Mester, F. Lindseth, DeepPrivacy: A Generative Adversarial Network for Face Anonymization, Lect Notes Comput. Sci. 11844 (2020) 565–578.
[43] N. Carlini, D. Wagner, Towards evaluating the robustness of neural networks, P IEEE S Secur. Priv. (2017) 39–57.
[44] J.W. Chen, L.J. Chen, C.M. Yu, C.S. Lu, Perceptual Indistinguishability-Net (PI-Net): Facial Image Obfuscation with Manipulable Semantics, 2021 Ieee/Cvf Conference on Computer Vision and Pattern Recognition, Cvpr 2021, (2021) 6474-6483.